Chem

CellPress

Review

Printable Solar Cells from Advanced Solution-Processible Materials

Sang-Hoon Bae,[1,2,3] Hongxiang Zhao,[1,2,3] Yao-Tsung Hsieh,[1,2,3] Lijian Zuo,[1,2,3] Nicholas De Marco,[1,2] You Seung Rim,[1,2] Gang Li,[1,4,*] and Yang Yang[1,2,*]

Considering the terawatt global demand for energy, studies on renewable energy resources are regarded as one of the most important issues. Among the available renewable energy resources, solar energy is a strong candidate because of its abundance and clean nature. Traditional solar cells are typically not cost effective for large-scale implementation given the high processing costs. Solution-processible solar cells have been of great interest among researchers over the past few decades in an effort to lower the costs of solar technologies because they are more affordable than conventional solar technologies. In this review, we provide an overview of the major solution-processible thin-film solar cell technologies by focusing on three representative fields: polymeric organic, inorganic chalcogenide, and organic-inorganic hybrid perovskite solar cells. This review describes the historical development, material properties, device structures, and highest performance of each technology under a single-junction configuration. In addition, the challenges of each technology and the future outlook are briefly discussed.

INTRODUCTION

Over the past few decades, global population growth and industrialization have created a more comfortable lifestyle in our society. Such commodities have been primarily a result of the use of fossil fuels for energy. Fossil fuels continue to dominate world energy consumption by providing approximately 80% of the world's energy resource as of 2015. However, fossil fuels have caused numerous environmental issues, such as increases in carbon dioxide, abnormal weather conditions, and air pollution.[1] Thus, there is a large global drive to advance research on renewable energy resources, including sun, wind, water, biomass, and geothermal energy, to replace these environmentally harmful fossil fuels.

Among the possible renewable energy resources, solar energy is one of the strongest candidates because of its abundance and environmentally friendly nature. Two major ways to utilize solar energy are through solar heating and the photovoltaic effect. In particular, the photovoltaic effect has become an attractive approach after the discovery of the silicon solar cell in 1954, which achieved approximately 6% power-conversion efficiency (PCE).[2] Unfortunately, this initial solar cell was much more expensive ($300/W) than a commercial plant (50¢/W). This prohibited the large-scale deployment of solar cells, especially for residential use. However, early solar cells did prove to be successful for specific applications where high cost was a less important factor, such as in space applications (e.g., communication satellites, orbiting astronomical observatories, and manned space laboratories). Even though the cost was not as important for space applications, it had a much smaller potential market size than that for terrestrial use. This drive for more affordable alternative types of

The Bigger Picture

In this review, we provide a general introduction to solar cells and representative solution-processible solar cell fields, including organic, inorganic, and organic-inorganic hybrid solar cells, which are useful in lowering the production cost of solar cells. The historical developments and properties of each type of solar cell are introduced, along with important discoveries. Also, we discuss the key challenges of each field and the recent progress.

Because we cover only solution-processible single-junction solar cells, we recommend articles dealing with non-solution-processible solar cells, such as Si and III-V solar cells, or some approaches beyond single junctions, such as tandem cells and light management. Combining these research efforts will further improve solar technology, allowing it to finally contribute to powering territorial applications.

solar cells is what led to the development of alternative solar cells, namely, thin-film solar cells. Such thin-film technologies included amorphous Si (a-Si),[3] cadmium telluride (CdTe),[4] and copper indium gallium diselenide (CIGS).[5] Although these thin-film technologies eliminated the use of high-cost wafers and also provided much lower material consumption, high-cost vacuum facilities and high-temperature processes were still required. This led to more recent interests in solution-processed thin-film solar cells, including organic[6] and chalcogenide-based[7] solar cells, dye-sensitized solar cells (DSSCs),[8] and hybrid perovskite solar cells (PSCs),[9] because of their lower production costs. Solution-processed solar cells have made low manufacturing costs possible through roll-to-roll processing, spin casting, high material utilization, aesthetic form factors, and more. Figure 1 depicts the significant steps conducted globally to realize solution-processible solar cell technologies over the recent years.

In this review, we will first provide a general introduction to the principles of solar cell operation and its fundamental limitations. Next, we will introduce three representative solid-state solution-processible solar cells: (1) organic polymer and (2) inorganic chalcogenide solar cells and (3) hybrid organic-inorganic PSCs. Another major solution-processed solar cell, the DSSC uses a liquid electrolyte and thus will not be covered in this review. Another field we will not cover is the colloidal-quantum-dot-based solar cell, which is also a very interesting field. This review will include the different structures, properties, historical development, and state-of-the-art designs of each technology. Finally, we will conclude with an outlook regarding the remaining challenges and future opportunities of these technologies.

FUNDAMENTALS OF SOLAR CELLS

Today's solar cell technologies are dominated by the p-n junction. In its simplest description, a solar cell consists of a junction of p- and n-type semiconductor materials that form a heterojunction and give rise to the photovoltaic effect. The photovoltaic effect is a direct process converting light energy into usable electrical energy. Solar irradiation has a wide energy range across its spectrum, i.e., photons have different energy associations on the basis of their frequency (or wavelength). Photons with energy larger than the band gap of the solar cell absorber material can excite electrons from the valence to the conduction band within that material, leaving holes behind in the states that electrons previously filled. These excited electrons are then able to move more freely as a result of this extra energy. However, the electrons will quickly lose this extra energy if they are not provided a driving force. To generate a potential difference through this process, the solar cell device must have built-in asymmetry to draw the photogenerated electrons and holes out of the absorber material. Otherwise, the excited electrons can quickly relax back to the ground state and recombine with the holes to give off thermal energy and essentially lose that absorbed photon energy. Once the electrons and holes are extracted into external circuitry via the potential difference, electricity can be produced (Figure 2A).

However, the current across a device with an applied forward bias (i.e., a higher voltage at the cathode than at the anode) is rather small without light shining on the device. In the dark, the saturation current is given by

$$J_{\text{dark}} = J_0\left(e^{\frac{qV}{nK_BT}} - 1\right), \qquad \text{(Equation 1)}$$

where J_{dark}, J_0, q, V, n, K_B, and T are, respectively, the dark current density, the reverse saturation-current density, the elementary electron charge, the applied bias voltage, the ideality factor, Boltzmann's constant, and the temperature. Under illumination, the device begins to generate power on the basis of the

[1]Department of Materials Science and Engineering, University of California, Los Angeles, Los Angeles, CA 90095, USA

[2]California NanoSystems Institute, University of California, Los Angeles, Los Angeles, CA 90095, USA

[3]Co-first author

[4]Present address: Department of Electronic and Information Engineering, Hong Kong Polytechnic University, Hung Hom, Kowloon, Hong Kong, People's Republic of China

*Correspondence: gangl@ucla.edu (G.L.), yangy@ucla.edu (Y.Y.)

http://dx.doi.org/10.1016/j.chempr.2016.07.010

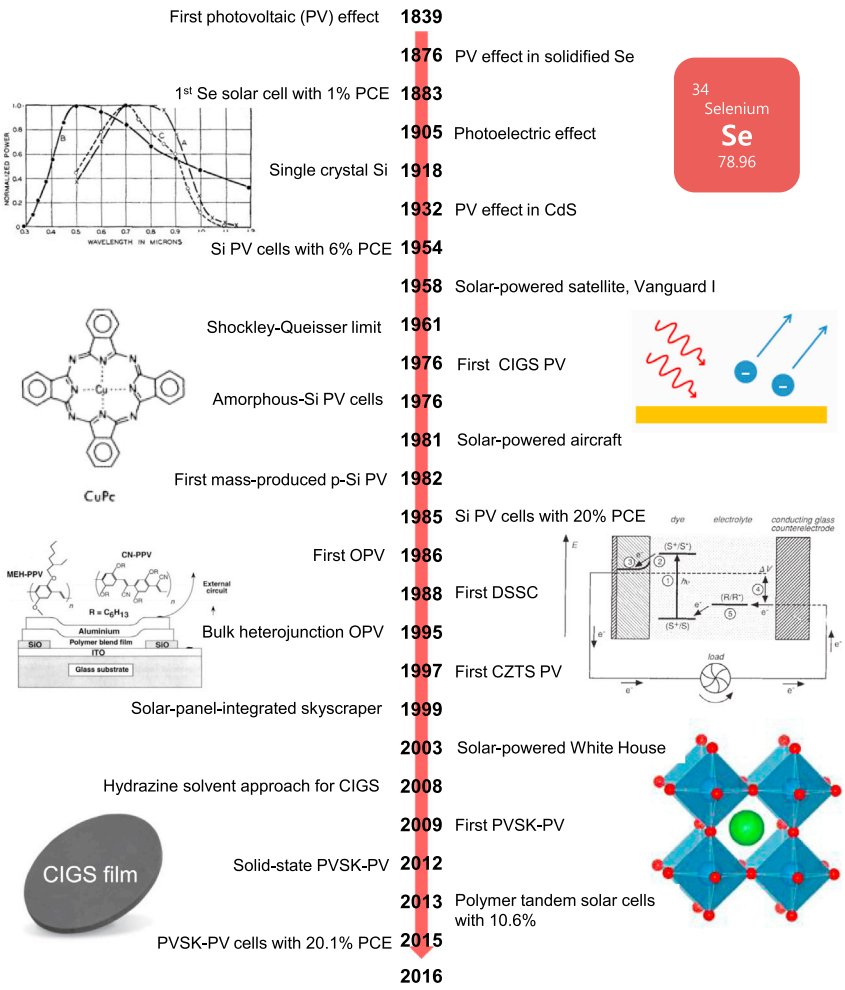

Figure 1. A Brief History of Solar Cells

(Left, top) Reprinted with permission from Chapin et al.[2] Copyright 1954 AIP Publishing.
(Left, second from top) Reprinted with permission from Tang.[6] Copyright 1986 AIP Publishing.
(Left, third from top) Reprinted by permission from Macmillan Publishers Ltd: Nature (Halls et al.[10]), copyright 1995.
(Right, third from top) Reprinted by permission from Macmillan Publishers Ltd: Nature (O'Regan and Grätzel[8]), copyright 1991.
(Right, bottom) Reprinted with permission from Chen et al.[11] Copyright 2015 Elsevier Inc.

photovoltaic effect and produce downward shifts in the J-V curve (Figure 2B, red curve $J_{dark} - V$). A maximum power point is achieved at the point where the product of the current density and the voltage is a maximum. At zero applied bias, there is a maximum current value called short-circuit conditions (J_{SC}), which is closely related to light absorption, exciton diffusion, and exciton dissociation. As the bias is increased, there is also a point where the voltage and current have maximum and minimum values, respectively, which is called the open-circuit voltage (V_{OC}). Knowing these parameters, we can determine what is called the fill factor (FF), which indicates how well charges are removed from the cell:

$$FF = \frac{J_{MP} \times V_{MP}}{J_{SC} \times V_{OC}}, \qquad \text{(Equation 2)}$$

where J_{MP} and V_{MP} are the maximum current density and maximum voltage, respectively. Lastly, given that the principle of solar cells is the conversion of light energy

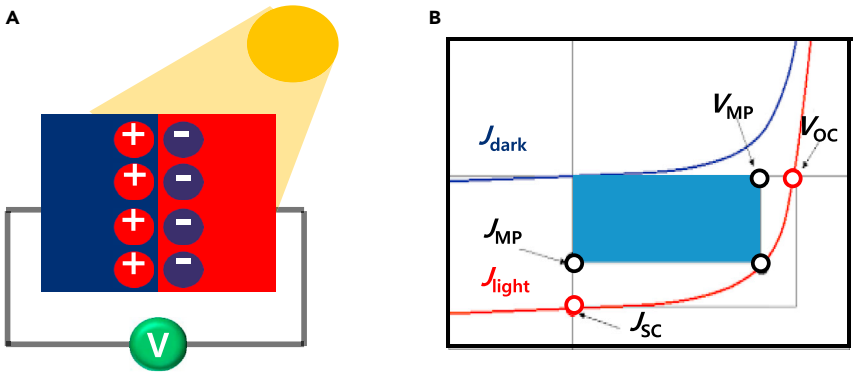

Figure 2. Schematic Illustrations for a Brief Introduction to Solar Cells
(A) Schematic illustration of the photovoltaic effect.
(B) Graph of light and dark voltage-current density.

into electricity, it is important to comprehend the PCE of devices (η). It can be expressed by the ratio of the maximum electrical power (P_M) to the total incident power (P_{in})[12]:

$$\mathrm{PCE} = \frac{P_M}{P_{in}} \times 100\% = \frac{V_{OC} \times J_{SC} \times \mathrm{FF}}{P_{in}} \times 100\% . \qquad \text{(Equation 3)}$$

Absorption and Absorption Coefficient

In a solar cell, we are concerned with how well photons are absorbed and can generate charge that can be extracted from the cell. It is important to quantify how effectively light can be absorbed in materials. The absorption coefficient is a representative term for determining how far incident light of a certain wavelength penetrates a material before being absorbed. The absorption coefficient is determined by the material and the wavelength of light (or photon energy), depicted in Figure 3A.[13] Semiconducting materials can demonstrate either a sharp increase in their absorption coefficient or a gradual increase in the absorption coefficient versus photon energy, as seen in Figure 3A. This can tell us whether the material has a direct or indirect band gap. A direct band gap corresponds to a sharp absorption onset, indicating that once the energy of the photon surpasses the energy of the band gap, absorption begins. Conversely, an indirect band gap corresponds to a gradual absorption onset, indicating that an additional factor to photon energy is necessary for absorption to occur, which is a phenomenon known as a phonon. The absorption coefficient is related to the extinction coefficient by

$$\alpha(\lambda) = \frac{4\pi k(\lambda)}{\lambda} . \qquad \text{(Equation 4)}$$

In addition, the absorption coefficient indicates that the light intensity drops as the light penetrates through a material (it is attenuated). Thus, it can be expressed in the form of the Beer-Lambert law:

$$I = I_0 e^{-\alpha x} , \qquad \text{(Equation 5)}$$

where I, I_0, and x, are the light intensity (~amount of photons) after the absorption, the initial light intensity, and the thickness of the material, respectively.[12]

Recombination and Diffusion Length

Recombination, which is a process where the excited electrons stabilize back down to their original state, is equally as important as the excitation by light absorption. Once the incident light shines onto the absorber layer, the number of minority

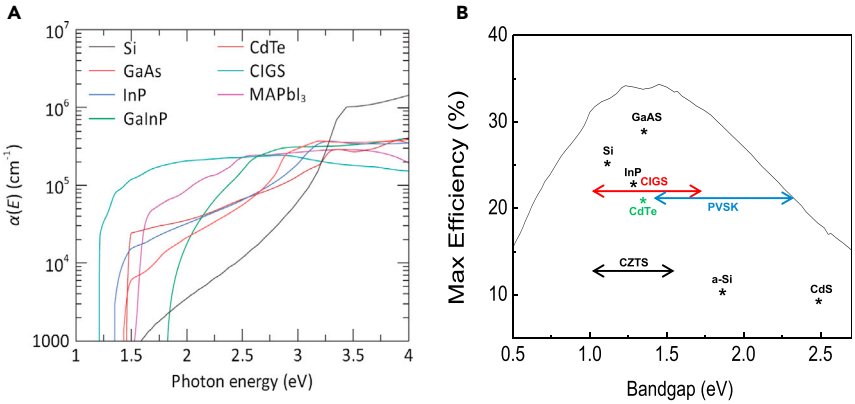

Figure 3. Optoelectrical Properties of Various Materials for Solar Absorbers

(A) Absorption coefficient of various materials. Reprinted by permission from Macmillan Publishers Ltd: npj Computational Materials (Alharbi et al.[13]), copyright 2015.

(B) Shockley-Queisser limit according to the band gap and materials. (The arrows show the range of band gaps achievable for compound semiconductors—CIGS, CZTS, and PVSK—through composition engineering.)

carriers increases, breaking the equilibrium. If not provided with an external driving force, excess minority carriers will then quickly decay back down to their equilibrium state, effectively annihilating a hole. The average time in which an electron remains in the excited state before recombination occurs is called the carrier lifetime (τ), which has the following expression for doped semiconductors:

$$\tau = \frac{\Delta n}{R}, \qquad \text{(Equation 6)}$$

where Δn and R are the excess carrier concentration and the recombination rate, respectively. Therefore, the distance that the excess carriers can diffuse within their carrier lifetime, called the diffusion length, can be determined through the expression

$$L = \sqrt{D\tau}, \qquad \text{(Equation 7)}$$

where D is the diffusivity. Because the carrier lifetime and diffusivity vary according to the material, these are critical factors to consider in the design of solar cells (Table 1).

There are three types of recombination mechanisms that can occur, namely, radiative recombination (i.e., spontaneous emission), Shockley-Read-Hall (trap-assisted) recombination, and a three-particle process called Auger recombination, which results when an electron and a hole recombine and give that extra energy to another electron, which thermalizes back to the conduction band edge. The latter is the dominate loss mechanism in indirect-band-gap materials, such as silicon and germanium.[12]

Shockley-Queisser Limit and Band Gap

William Shockley and Hans J. Queisser studied the theoretical thermodynamic upper limit of solar cell efficiency, which is called the Shockley-Queisser limit or the detailed balance limit.[14,15] The Shockley-Queisser model has four commonly accepted assumptions:

1. One incident photon generates one electron-hole pair.
2. Photons with energy larger than the band gap of photoactive materials are completely absorbed; those with lower energy than the band gap do not generate charge carriers.

Table 1. Diffusion Length of Each Material

Material	Diffusion Length (μm)
Si	200
GaAs	1
InP	3
CIGS	2
CdTe	3
CZTS	0.3
$MAPBI_3$	300

3. Radiative recombination is the only recombination loss.
4. The incident light is neither concentrated nor anisotropic.

The Shockley-Queisser model predicts the maximum efficiency of a single-junction solar cell as a function of the band gap of the material, as shown in Figure 3B.

SOLUTION-PROCESSIBLE THIN-FILM SOLAR CELLS

The main advantage of solution-processible solar cells is that they do not require vacuum or high-temperature processes. In this section, we provide a concise review of the three representative solution-processible solar cell fields—organic polymer and inorganic solar cells and hybrid PSCs.

Organic Polymeric Solar Cells

Organic polymeric photovoltaic (OPV) technology has emerged as a promising direction for renewable energy given its advantages in synthetic variability, low-temperature and low-cost fabrication, lightweight nature, and mechanical flexibility.[16–18] Conjugated molecules and polymers in organic semiconductors are constrained by intermolecular forces, whereas in inorganic semiconductors, atoms are covalently or ionically bonded. π-electrons are delocalized within each conjugated molecule as a result of π-conjugation of molecular orbitals formed by p_z atomic orbital overlaps, mainly sp^2 hybridization. As a result, charge carriers can move relatively freely along the conjugated backbone. Hopping between molecules, on the other hand, is more difficult. However, the carrier mobility of organic semiconductors is much lower than that of inorganic semiconductors.[19,20] The electron-hole pairs in organic polymers are tightly bound Frenkel-type excitons as a result of the low dielectric constants (ε_r = 2–4) of organic materials. Binding energies are typically in the range of 0.3–1 eV. Conversely, a Wannier-type exciton, which is a free electron-hole pair at room temperature, is found in inorganic materials with around 30 meV of binding energy. Organic semiconductors are thus better described in molecular orbital language than classical band theory. The band gap of the material is determined by the difference between the lowest unoccupied molecular orbital (LUMO), corresponding to a conduction-band minimum, and the highest occupied molecular orbital (HOMO), which corresponds to a valence-band maximum. P-type (or electron-donor) materials have a relatively high HOMO level and are more likely to be p-doped and transport holes. N-type (or electron-acceptor) materials have a relatively low LUMO level and are more likely to be n-doped and transport electrons.

Conjugated polymers are constructed by means of C–C bond formation between each two unsaturated carbon atoms in two monomers. In order to achieve this, two functionalized aryl groups take part in the cross-coupling polymerization,

facilitated by a transition-metal catalyst. One arene is substituted with a leaving group, typically a halogen, whereas the other has -MgX (Kumada-Corriu), -SnR_3 (Stille), and -$B(OR)_3$ (Suzuki-Miyaura).[21–23] Generally speaking, the reaction begins with oxidative addition, where the R–X bond is broken and the transition metal is oxidized. Next, transmetallation occurs with a main-group organometallic nucleophile. Finally, after reductive elimination, a transition-metal catalyst is generated in situ, and a new C–C bond forms between two arene groups. The advantage of transition-metal catalysis includes mild reaction conditions, stereoselectivity, and regioselectivity. The most popular and efficient polymerization methods are Stille and Suzuki coupling reactions.

While working at Kodak, Tang opened up the field of modern OPV technology by introducing donor and acceptor molecules in a two-layered structure,[6] which successfully led to efficient photogeneration of carriers in organic absorbers. The first successful OPV device had a PCE of around 1%, which was reported in 1986. In the early 1990s, there was another OPV breakthrough—the solution-processible polymer solar cell. This was made possible by a few seminal scientific discoveries: (1) Heeger et al. at the University of California, Santa Barbara, reported ultrafast charger transfer from a polymer donor, poly[2-methoxy-5-(2′-ethylhexyloxy)-*p*-phenylene vinylene] (MEH-PPV), to C60, which occurred on the timescale of tens of femtoseconds, indicating very efficient charge separation within the material system;[24] and (2) Yoshino et al. in Osaka observed changes of interband and intraband optical absorption and photoluminescence quenching when they blended poly(3-hexylthiophene-2,5-diyl) (P3HT) with C60. This provided another strong piece of evidence of charge transfer between the two materials. These discoveries were a huge step in OPV history, and fullerene derivatives are still widely used as an electron acceptor today. Later studies showed that the exciton diffusion lengths were only around 10 nm.[25,26] To avoid exciton recombination, the thickness for planar two-layered OPV films had to be much thinner (~20 nm), which is rather inefficient for absorbing sufficient sunlight. Furthermore, the interfacial area between donor and acceptor materials in bilayer structures was limited in achieving efficient charge separation.

In 1995, a new type of solar cell—the bulk heterojunction (BHJ) OPV solar cell—was successfully achieved independently by Yu et al. on polymer (donor):fullerene (acceptor) systems[27] and by Halls et al. on polymer:polymer systems.[10] This bicontinuous donor-acceptor network provided efficient carrier transport in donor and acceptor domains, and the large interfacial area ensured that efficient charge separation occurred at the interface. The carriers were then collected efficiently by two electrodes to complete the circuit. Compared with planar structures, BHJ devices have increased the PCE greatly, and they are the dominant OPV structure today.

The design and synthesis of new absorber materials for OPV technology have been a hot topic for chemists during the last two decades. One of the earliest and most successful polymers for organic electronic applications is poly[2-methoxy-5-(2′-ethylhexyloxy)-*p*-phenylene vinylene] (MEH-PPV), which was developed by Wudl and Srdanov.[28] Synthetic methods of MEH-PPV include the Wessling and Glich routes, where mild polymerization conditions and high molecular weights were obtained through the second route.[29,30] Improvement of MEH-PPV was limited by its relatively low hole mobility and wide band gap. Another important polymer in the OPV history is P3HT, which was first reported in 1992.[31] P3HT has a band gap of 2.0 eV, which is smaller than that of MEH-PPV. This enabled further absorption of the solar spectrum. Along with its high hole mobility and regioregularity, P3HT could reach PCEs of 4%~5%.[32] Until now, much attention has been given to modifying the device

structure, film morphology, and electron acceptor in P3HT-based devices. The PCE of P3HT-based OPV devices can now reach up to 7% with the use of acceptors with a shallower LUMO.[33] However, the band gap of P3HT is still too large and the HOMO level is still too high, such that photon absorption in the near-infrared (NIR) region is poor and the open circuit voltage is low.

Five synthetic approaches involve band gap engineering: (1) stabilizing quinoid resonance structures, which have a lower band gap than their aromatic counterpart; (2) rigidifying conjugated aromatic rings such that π-electrons can delocalize; (3) incorporating electron-donating or electron-withdrawing functional groups onto the backbone; (4) copolymerizing electron-rich donors and electron-deficient acceptors in an alternating manner; and (5) constructing conjugated side chains. For more detailed polymer design principles, see the excellent review articles by Li[34] and Cheng et al.[35] Here, we intend to give a concise summary of representative new polymers designed according to the guidelines above. Figure 4 shows the chemical structures of some of the representative donor polymers.

A lower-band-gap poly(*N*-alkyl-2,7-carbazole) derivative (PCDTBT) was reported by Blouin et al.[36] with a low HOMO level of −5.50 eV and a V_{OC} as high as 0.89 V, which reached a PCE value of 3.6%. However, its 1.88 eV optical band-gap was still not small enough to harvest NIR photons. Later, another series of polymers were synthesized, namely, poly[(4,4-bis(2-ethylhexyl)-cyclopenta-[2,1-b;3,4-b′]dithiophene)-2,6-diyl-*alt*-2,1,3-benzothiadiazole-4,7-diyl] (PCPDTBT) and an improved version incorporating a silicon atom to replace carbon, called poly[(4,4′-bis(2-ethylhexyl)dithieno [3,2-b:2′,3′-d]silole)-2,6-diyl-*alt*-(2,1,3-benzothiadiazole)-4,7-diyl] (PSBTBT),[37,38] both of which have a small band gap of around 1.5 eV and show a photo-response up to 850 and 820 nm, respectively. One of the most famous OPV polymers after P3HT is PTB7, which was first published in 2010 and reached a PCE of 7%–8%.[39] The polymer PTB7 is composed of (1) a thieno[3,4-b]-thiophene (TT) acceptor unit[40] with a quinoid structure to realize its low band gap, (2) a benzo[1,2-b;4,5-b′]dithiophene (BDT) unit[41] to provide a large planar molecular structure, and (3) an electron-withdrawing F-atom at three positions to lower the HOMO level and raise the V_{OC}. The band gap was approximately 1.65 eV with a HOMO level of −5.15 eV.

Polymers with low band gaps of ~1.4 eV are useful not only in traditional single-junction OPV devices but also in tandem OPV devices. These polymers can be used for improving efficiency and are also highly transparent, which is useful for unique OPV applications. The two most representative low-band-gap polymer families are (1) diketopyrrolopyrrole (DPP), which was first introduced in 2008 by Janssen, and (2) benzothiadiazole (BT). Our group carried out a systematic investigation of the planar BDT unit and DPP-based low-band-gap polymers. Replacing the oxygen atoms attached to the BDT unit with thiophene moieties to form the thienylbenzodithiophene (BDTT) unit shifted the HOMO level of the resulting PBDTT-DPP down (−5.30 versus −5.16 eV) to increase the V_{OC}. A 6.5% PCE was achieved in a single-junction configuration, and a record efficiency of 8.62% for the tandem polymer solar cell was achieved and certified by the National Renewable Energy Laboratory (NREL) in 2012 when P3HT:ICBA was used as the other subcell.[42] Regarding BT, our group co-polymerized an asymmetric, strong, electron-rich dithieno[3,2-b:2′,3′-d] pyran (DTP) unit with a strongly electron-deficient difluorobenzothiadiazole (DFBT) unit, demonstrating a regiorandom polymer (PDTP-DFBT, band gap = 1.38 eV) with excellent photovoltaic properties. Single-junction devices reached an efficiency of 8.0%, and tandem polymer solar cells fabricated with P3HT and PDTP-DFBT achieved 10.6% efficiency, which were certified by NREL.[43]

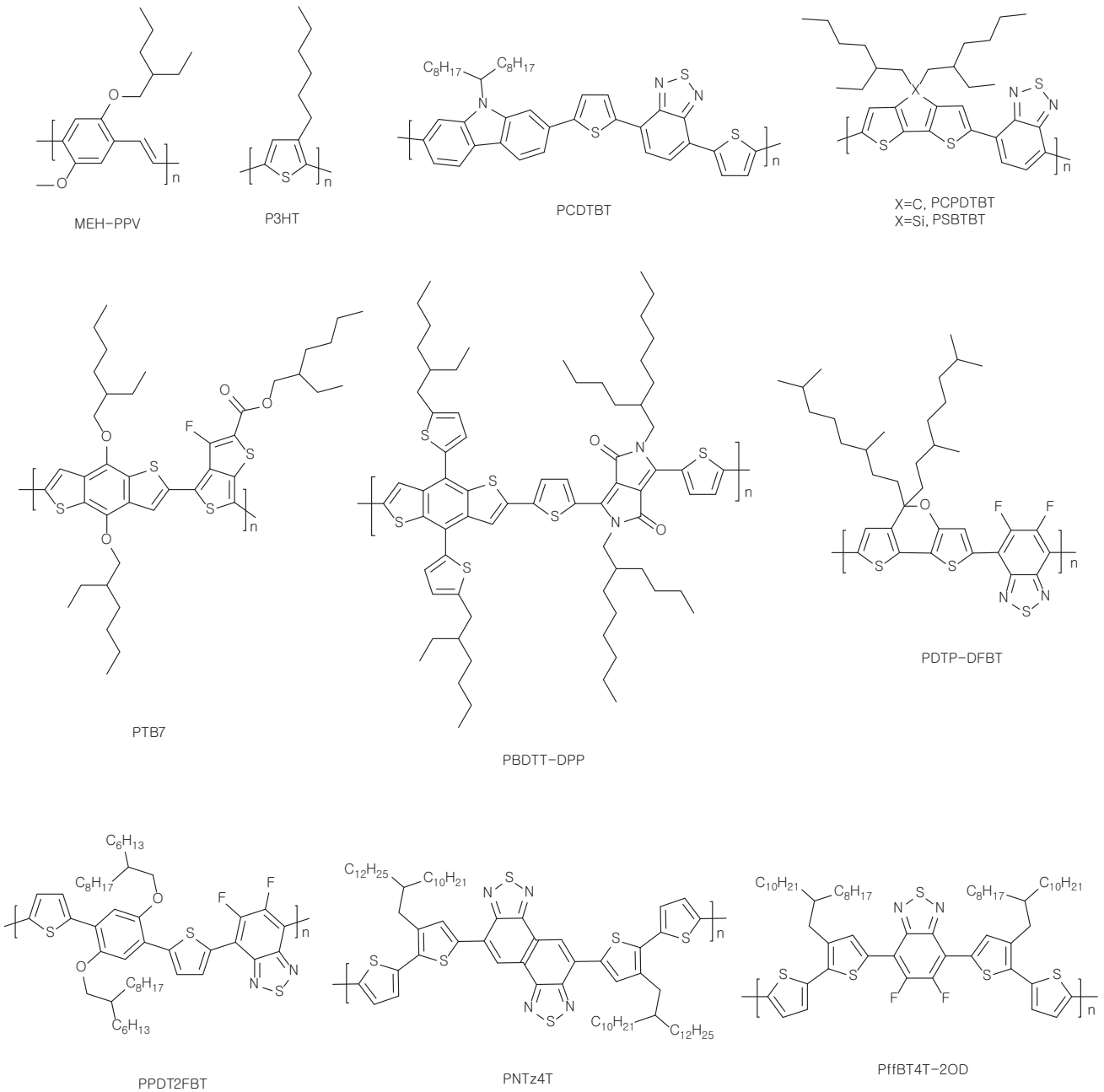

Figure 4. Chemical Structures of Representative Donor Polymer Molecules

Recently, various other polymer structures have shown huge potential for achieving higher efficiency. Poly[(2,5-bis(2-hexyldecyloxy)phenylene)-*alt*-(5,6-difuoro-4,7-di(thiophen-2-yl)benzo[c]-[1,2,5]thiadiazole)] (PPDT2FBT) was reported with a 9.4% PCE.[44] Through intra-molecular interactions, the backbone has better planarity and intermolecular ordering. The fluorine atoms not only take part in the noncovalent attractive interaction but also improve hole mobility. The naphtho[1,2-c:5,6-c′]bis[1,2,5]thiadiazole (NTz)-based polymer PNTz4T has shown great crystallinity as a result of the strong π-π stacking interactions between the backbones.[45] Interestingly, the high efficiency was achieved with a thick active layer of around

300 nm. The HOMO level of the polymer is relatively high, around −5.14 eV, making the $E_g - V_{OC}$ offset too large, and much photon energy is wasted. Another recent promising family of polymers, synthesized by Chen et al.,[46] is based on 5,6-difl uorobenzothiadiazole (DFBT) as the acceptor unit and quarterthiophene as the donor unit and shows an efficiency of 7.64%. It was soon shown that the potential of this type of polymer can be significantly improved by decreasing the length of the side chains and tuning the morphology by controlling aggregation. Liu et al. reported the polymer poly[(5,6-difluoro-2,1,3-benzothiadiazol-4,7-diyl)-*alt*-(3,3000-di(2-octyldodecyl)-2,2′;5′,2″;5″,2‴-quaterthiophen-5,5‴-diyl)] (PffBT4T-2OD) to have an efficiency as high as 10.8% through better morphology control.[47] Later on, the same group switched PffBT-2OD with slightly longer side chains to get an even higher efficiency of 11.7%, which is by far the highest reported. Notably, they used hydrocarbon solvents instead of halogenated solvents to process polymer films.[48] Another advance to be noted in the OPV field is the non-fullerene acceptor. By carefully choosing the combination of a polymer donor and small-molecule acceptor, Zhao et al. reached a PCE of 11.21%, which is among the highest efficiencies in OPV technology.[49]

Understanding and controlling polymer-blend morphology plays a critical role in realizing high-performance polymer solar cells. Efforts to control morphology in solar cells based on the blend of P3HT and phenyl-C61-butyric acid methyl ester (PCBM) (P3HT:PCBM solar cells), such as thermal annealing, solvent annealing, additives, etc., have significantly deepened the understanding of OPV technology. Figure 5 shows examples of common morphology-characterization results from two very important polymer-blend systems: the classical P3HT:PCBM and PTB-7:PCBM systems. Figure 5A shows that tapping-mode atomic force microscopy (AFM) phase images can provide nanoscale material contrast for solvent-annealed high-crystalline P3HT:PCBM films.[50] Transmission electron microscopy (TEM) is another powerful tool in OPV research. Figure 5B shows the bright-field TEM image of a PTB-7:PCBM film formed via a solvent-additive method of optimizing donor-acceptor morphology.[39] This represented the first time in OPV history that 7%–8% efficiency was achieved. Grazing-incidence X-ray diffraction is also useful for detecting molecular-level details of crystalline structures in BHJ thin films. A synchrotron beamline with a high X-ray photon flux and collimation is very helpful for acquiring accurate structural information. In Figure 5C, solvent-annealed P3HT:$PC_{61}BM$ films with higher vibronic π-π stacking peaks in absorption were examined with a synchrotron X-ray source. The prominent (n00) diffraction peaks indicate high crystallinity with a dominant edge-on chain orientation. The result also shows a reduction in polymer inter-chain spacing through the solvent-annealing approach (from 16.9 Å in fast-grown film to 16.3 Å in solvent-annealed film). Figure 5D is the grazing-incidence wide-angle X-ray scattering (GIWAXS) image of PTB-7:PC61BM films casted from a CB (chlorobenzene):DIO (diiodooctane) additive, indicating that the polymer packing is dominantly face-on.[51]

The OPV morphology is relatively complicated and strongly dependent on the material system. Other representative characterization techniques also include electron tomography, energy-filtered TEM, near-edge X-ray absorption fine-structure spectroscopy, resonance soft X-ray scattering, specular X-ray reflectivity, and more.[17]

The morphology of the film in an OPV device is strongly connected to the type of polymer material used. Within the same polymer family sharing the same backbone, the effectiveness of polymer still critically depends on carefully choosing the polymer side chains, which ensure great inter-chain interaction and crystallinity and

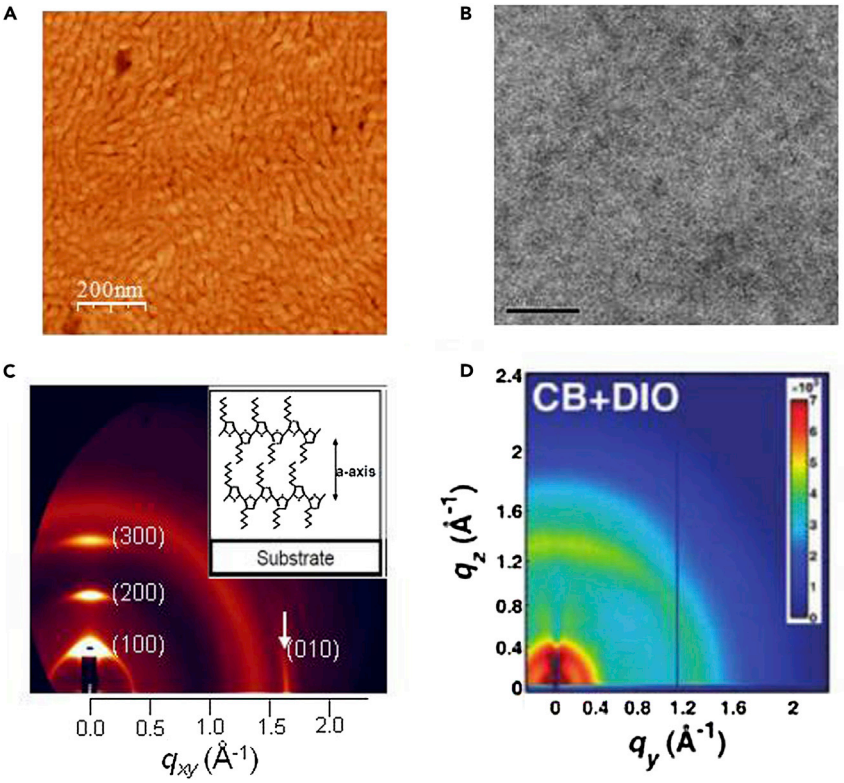

Figure 5. Common Morphology Characterization of Organic Polymer Solar Cells

(A) Tapping-mode AFM phase image of a solvent-annealed high-crystalline P3HT:PCBM solar cell. Note the polymer bundle size ~20 nm. Scale bar represents 200 nm. Reprinted with permission from Li et al.[50] Copyright 2007 John Wiley & Sons Inc.

(B) Bright-field TEM image of PTB-7:PC61BM film casted from CB as a major solvent with DIO as an additive. Scale bar represents 200 nm. Reprinted with permission from Liang et al.[39] Copyright 2010 John Wiley & Sons Inc.

(C) GIWAXS results of solvent-annealed high-crystalline P3HT:PCBM film. Reprinted with permission from Li et al.[50] Copyright 2007 John Wiley & Sons Inc.

(D) GIWAXS image of PTB-7:PC61BM films casted from CB as major solvent with DIO as an additive. Reprinted with permission from Chen et al.[51] Copyright 2011 American Chemical Society.

thus lead to high performance. Finding suitable side chains is thus an active research area in the OPV field. In addition, there is strong interest in (1) making novel p-type polymers compatible with a series of n-type materials to enhance V_{OC} and (2) designing new n-type molecules or reducing the cost of n-type molecules (e.g., non-fullerene acceptors) to improve the existing OPV technologies.

Despite the advantages mentioned earlier, typical synthesis methods (e.g., Stille and Suzuki coupling reactions) also have some drawbacks. First, stannyl is toxic, and removing traces of tin by-products from the reaction mixture is not easy.[52] Second, aryl halides react sluggishly in Suzuki coupling, and by-products can be generated by solvent-dissolved oxygen.[53] Besides that, these reactions also require extra synthetic steps and compounds (such as SnR_3), which are not stable. Recently, a new polymerization method, namely direct (hetero)arylation, has been used to synthesize polymers such as P3HT and PCPDTBT, leading to higher performances and potential ways to avoid previous drawbacks.[54,55] The catalytic cycle of these transition-metal-catalyzed reactions is shown in Figure 6.

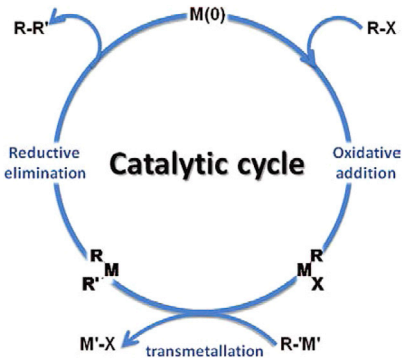

Figure 6. Catalytic Cycle of Transition-Metal-Catalyzed Reactions
Reprinted with permission from Cheng et al.[35] Copyright 2009 American Chemical Society.

Solution-Processed Inorganic CIGS/CZTS Thin-Film Solar Cells

Chalcogenide compounds are the main group of inorganic semiconductor materials that can compete with the fully fledged amorphous and polycrystalline silicon-based solar cells. At the early stage, CdTe was considered a great candidate for a thin-film absorber material with lower costs than Si-based solar cells. However, the toxicity of cadmium became the main hindrance of its application. In this section, we focus on two solution-processible chalcogenide compounds—copper indium gallium selenides (CIGS) and copper zinc tin sulfide (CZTS)—that have significantly less toxicity and far better device performance than Si- and Cd-based solar cells, encouraging the capability for large-scale application of solar-energy conversion (Table 2).

CIGS solar cells were developed from the technology of copper indium diselenide ($CuInSe_2$ [CIS]) solar cells. CIS exists in a chalcopyrite crystal structure that is stable from room temperature to 810°C. Initially, CIS was used as an absorber material because of its large absorption coefficient ($\sim 10^4$ cm^{-1}) and direct band gap.[56] However, CIS has a band gap of merely 1.02 eV, which is lower than the ideal value for solar cells. This drawback led to further modification of the compound, whereby gallium was doped into the CIS structure for increasing energy band gap, which brought the advent of $CuIn_xGa_{(1-x)}Se_2$ (CIGS). CIGS is a higher-band-gap quaternary alloy with the I-III-VI_2 chalcopyrite crystal structure and is composed of copper, indium, gallium, and selenium (Figure 7A).[57] Replacing gallium with indium allows continuous alteration of the CIGS band gap, which ranges between 1.02 eV for CIS and 1.68 eV for $CuGaSe_2$. CIGS has a high absorption coefficient of $\sim 10^5$ cm^{-1}, and its electronic property is strongly related to intrinsic defects and stoichiometry fluctuation inside the materials. It has been observed that the p-type CIGS with a slightly copper-deficient composition is suitable for photovoltaic applications. Achieving superior photovoltaic-device performance requires that the Ga/(Ga + In) ratio be controlled within 0.25–0.35. In this regard, the corresponding energy band gap will be 1.1–1.24 eV, which gives much better potential than the pure CIS system.

Normally, fabricating high-efficiency CIGS solar cells involves depositing polycrystalline CIGS on Mo-coated glass. For promoting the grain growth of polycrystalline CIGS, the deposited film is exposed to selenium vapor or selenium hydride gas (H_2Se) at high temperatures (above 500°C) in a process called selenization. This thermal treatment is also commonly applied for sintering and grain growth of other chalcogenides. At present, the highest-performing CIGS solar devices, which were

Table 2. Properties of Inorganic Thin-Film Solar-Active Materials

	Si	CdTe	CIGS	CZTSSe
Best PCE (%)	25.6	21	22.3	12.6
Carrier lifetime	~1 ms	~350 ns	~10 ns	~8 ns
Absorption coefficient (cm^{-1})	$\sim10^4$	$>10^4$	$>10^5$	$>10^4$
Direct band gap	X	O	O	O
Band gap (eV)	1.1	1.44	1.02–1.68	1.0–1.5

fabricated by a co-evaporation process in 2015 by Solar Frontier,[60] have reached PCEs of above 22.3% on a laboratory scale.

Even though high-quality CIGS films have been fabricated by vacuum-based processes, the technology thus far is not as competitive as originally thought. Therefore, a wide variety of novel solution-based processes aimed at further reducing the manufacturing costs and improving device performance have been explored intensively over the past few years.[7,61–64] These techniques include spray pyrolysis, electrochemical deposition, and nanoparticle-precursor deposition. However, few of these techniques are able to provide sufficient device performance to match that of co-evaporation. These solution-based processes have common constraints in (1) the incorporation of impurities from the precursor solutions, such as chlorine, carbon, and oxygen; (2) the obligation of selenization or sulfurization at high temperatures (above 500°C); and (3) the difficulties in adjusting the Ga/In ratio in a uniform and precise manner. In 2008, researchers at the IBM Thomas J. Watson Research Center established a hydrazine-based solution process to better avoid these constrains by using post-deposition selenization with better material utilization. The cross-sectional scanning electron microscopy (SEM) image of CIGS is shown in Figure 7C.[58] Hydrazine was utilized as a solvent to dissolve the metal chalcogenides, thereby forming a molecular solution to ensure the high uniformity and facile composition control of the CIGS film.[65] This approach revived the application of solution process in chalcogenide-based solar cells.

Other popular inorganic thin-film absorbers originating from CIGS—Cu_2ZnSnS_4 (CZTS) and $Cu_2ZnSn(S_x,Se_{1-x})_4$ (CZTSSe)—are aimed at removing the toxicity component of cadmium and scarcity of tellurium, indium, gallium, and selenium in CdTe and CIGS absorber materials. By substituting indium and gallium with zinc and tin and substituting selenium with sulfur, the copper-based I_2-II-IV-VI_4 quaternary kesterite compound CZTS and its relative compounds CZTSSe have been considered other alternatives to compete with CdTe and CIGS (Figure 7B).[66–68] Because of their competitive absorption coefficient ($\sim10^{-4}$ cm^{-1}) and adjustable optical band gap (1.0–1.5 eV), these earth-abundant and non-toxic kesterite-based materials have quickly become some of the most promising candidates for thin-film solar cell technologies.

The kesterite structure allows for various types of vacancies, interstitials, and antisites such that discrete energy level(s) could emerge and give rise to p-type conductivity in CZTS materials. It has been confirmed that this intrinsic p-type doping is highly sensitive to stoichiometry variation.[66,69,70] Compared with CIGS, CZTS has a much narrower single-phase composition. As a consequence, it becomes crucial to control the phase formation during the thermal treatment to preserve the phase purity and further acquire high-performance CZTS devices. Also, it is known that all of the high-efficiency devices reported in the literature exist within a small

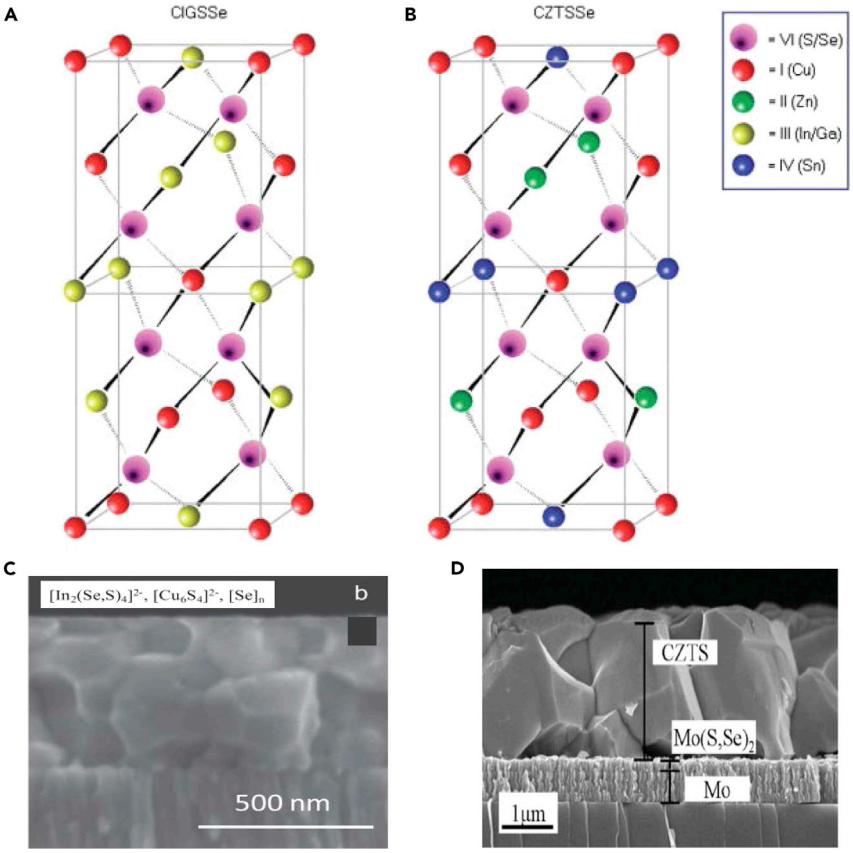

Figure 7. Schematic Illustrations and Cross-sectional SEM Images of Two Inorganic Chalcogenide Compounds

(A) Chalcopyrite crystal structure of CIGS.

(B) Kesterite crystal structure of CZTS. Reproduced from Polizzotti et al.[57] with permission of the Royal Society of Chemistry.

(C) CIGS film by hydrazine treatment to induce high uniformity and facile composition control. Scale bar represents 500 nm. Reprinted with permission from Chung et al.[58] Copyright 2013 Elsevier Inc.

(D) CZTS film of a 12.6% record device using a hydrazine pure-solution approach. Scale bar represents 1 μm. Reprinted with permission from Kim et al.[59] Copyright 2014 John Wiley & Sons Inc.

stoichiometric range, i.e., copper poor (Cu/[Zn + Sn] = 0.8∼0.9) and zinc rich (Zn/Sn = 1.1–1.4). This off-stoichiometry range is favored because of the volatile nature of its elemental constituents and related binary phases generated during the CZTS film formation.[69]

Copper-poor and zinc-rich compositions of CZTS(e) provide two main benefits for approaching high-efficiency solar devices. The first advantage is proper secondary-phase precipitation. It can effectively prevent shunting paths by inducing the precipitates of the ZnS(e) phase during the CZTS(e) grain growth. The wider-band-gap ZnS(e) phase will impede the formation of other, more conductive phases, such as SnS(e), Cu_2S(e), and Cu_2SnS(e). Second, this off-stoichiometry compound encourages the formation of benign defect clusters [V_{cu} + Zn_{Cu}]. It has been calculated that the defect cluster [V_{cu} + Zn_{Cu}] has a relatively lower formation energy than other defects. More importantly, [V_{cu} + Zn_{Cu}] contains a shallower acceptor level so that it can effectively reduce charge-carrier recombination at deep levels

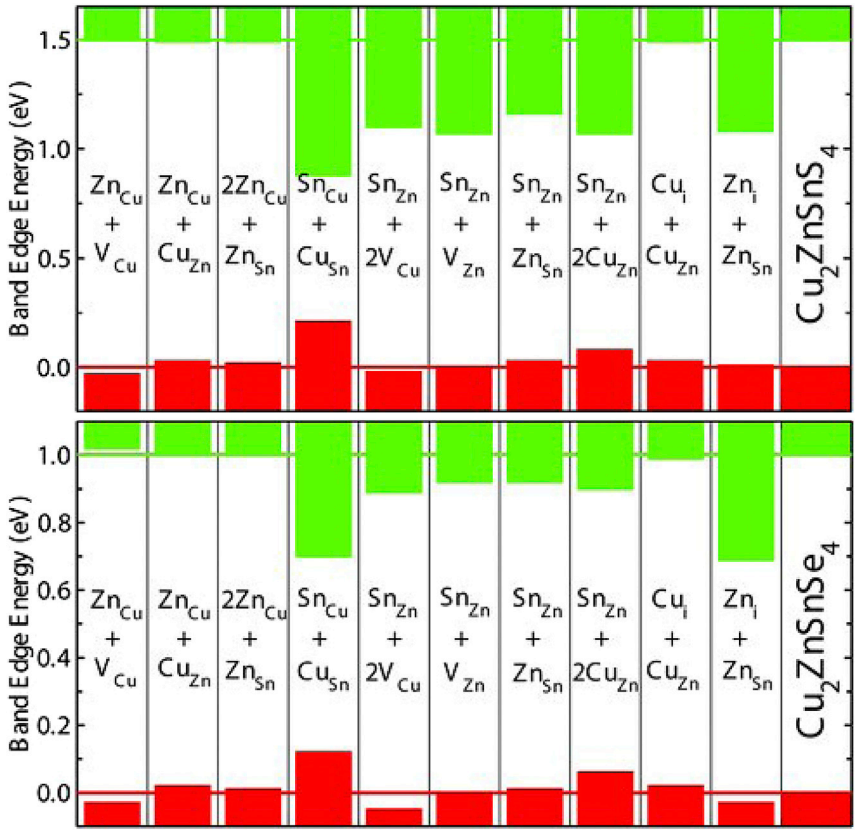

Figure 8. Calculated Band Shifts

The modeling result shows that the valence and conduction bands shift by several defect clusters in CZTS (top) and CZTSe (bottom) with a defect concentration of one defect cluster in a 128-atom supercell. Reprinted with permission from Chen et al.[69] Copyright 2013 John Wiley & Sons Inc.

and mid-gap states within the p-type kesterite compounds. One feature of CZTS compounds is that they have better defect tolerance, which offers their potential for solution process. As shown in Figure 8, CZTS and CZTSe can have several different defect-cluster possibilities. The formation of these defect clusters depends on chemical-potential variation, which is directly related to the elemental composition ratio. The band-edge shift is sensitive to the population of defect clusters and therefore affects the electron and hole transport. With precise composition control, there will be less vulnerability in utilizing the solution process for the CZTS(e) absorbers, in which the benign defects dominate.[69]

At present, the highest efficiency of CZTSSe solar cells is a PCE of 12.6%, which IBM achieved by using the hydrazine-based solution process shown in Figure 7D.[59] However, because it is known that hydrazine is highly toxic and explosive, many research groups continue to investigate other alternative solution processes by using much safer and facile solvents. Given the type of precursor solutes, the precursor solution must be processed with a final annealing for grain growth, as shown in Figure 9. A prevalent approach is to synthesize quaternary colloidal CZTS nanocrystals by thermolysis techniques.[67,71] As-designed CZTS nanocrystals (with the same composition as the target phase) are coated with organic ligands, such as oleylamine, to prevent aggregation and form a stable solution in nonpolar solvents. Besides colloidal quaternary nanocrystals, a precursor solution composed of binary and

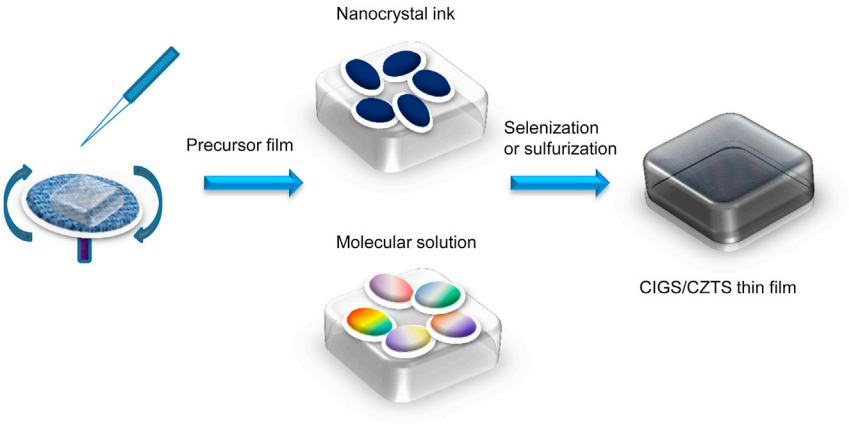

Figure 9. Schematic Diagram of the Solution Process for CIGS/CZTS Absorber Layers
The solution process includes intermediate annealing for the formation of precursor film and high-temperature annealing for grain growth.

ternary nanocrystal metal sulfides, which can facilitate the composition control by a simple mixing of precursors with recognized quantities, has also been proposed. The ligands capping the nanocrystal surfaces are normally considered undesired impurities and can ideally be removed through thermal treatment. For another approach using molecular species, dimethyl sulfoxide, methanol, and 2-methoxyethanol have been proposed as solvents for dissolving copper, zinc, and tin containing salts and thiourea sequentially.[72,73] Without multiple synthesis and washing steps for making nanocrystal inks, this molecular solution route is easier for fabrication and composition control. More importantly, it offers a facile system for studying the effects of dopants and surface ligands.

The main challenge of kesterite-based solar cells is their larger V_{OC} deficit. The V_{OC} of the champion CZTSSe device reaches only 62.6% of the Shockley-Queisser limit, but its J_{SC} and FF can get to above 80% of the Shockley-Queisser limits. Speeding up the progress requires that the defects in the kesterite compound and grain boundaries be eliminated. The control of defect generation highly counts on the development of deposition techniques.

Organic-Inorganic Hybrid PSCs

The organic-inorganic hybrid PSC is composed of an organic-inorganic hybrid material adopting the perovskite crystal structure.[74,75] The perovskite structure can be described as ABX_3, where A is an organic (or inorganic) cation (e.g., methylammonium [MA^+], formamidinium [FA^+], Cs^+, etc.), B is a metal cation (e.g., Pb^{2+}, Sn^{2+}, etc.), and X is an anion (e.g., I^-, Br^-, Cl^-, SCN^-, etc.). Figures 10A–10C show the typical perovskite crystal structure, where [BX_6] octahedra are stabilized with the A cation, and the B-X bond determines the optoelectronic properties of the perovskite structure.[11] To stabilize perovskite structures, the ionic radius of the A, B, and X ions must coordinate with each other within a range determined by the tolerance factor t of 0.85–1.11 ($t = (R_A + R_X)/\sqrt{2}(R_B + R_X)$, where R_A, R_B, and R_X are, respectively, the ionic radius of A^+, B^{2+}, and X^-).[77] Non-ideal cubic structures can form as a result of size effects and other factors, leading the octahedral to tilt. As a result, different phases of perovskites can form at different temperatures (Figure 10D), and the optoelectronic properties of different phases can vary significantly.[76] On the other hand, adjusting the composition of these A, B, and X components can create perovskite structures from zero to three dimensions (Table 3).[78,79]

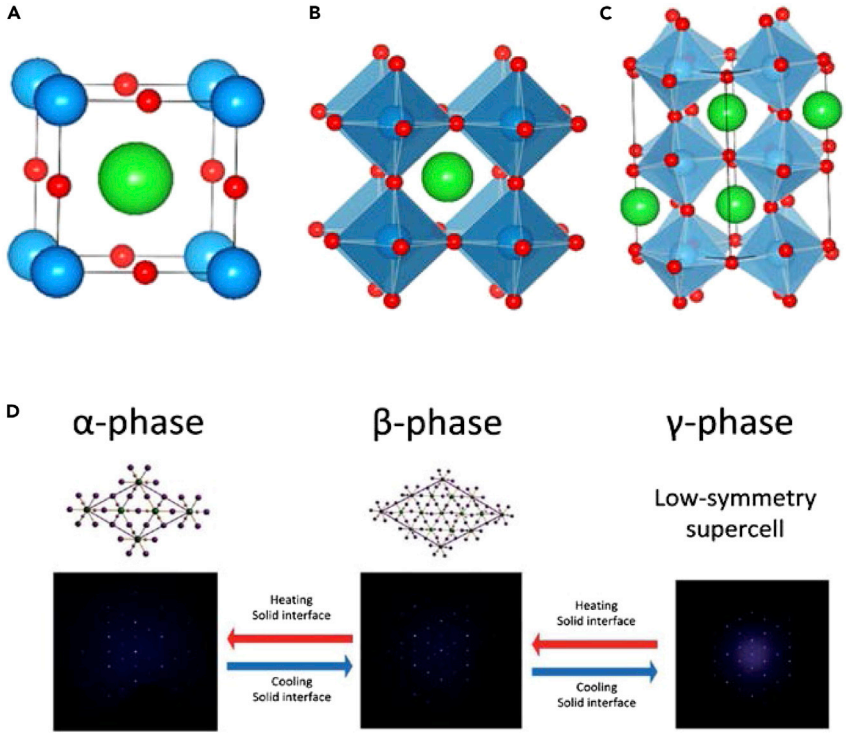

Figure 10. Perovskite Unit Cells and Phases

(A) A cations (blue) occupy the lattice corners, B cations (green) occupy the interstitial site, and X anions (red) occupy lattice faces.

(B) An alternative view depicts B cations assembled around X anions to form BX_6 octahedra, given that B-X bonds are responsible for determining electrical properties.

(C) BX_6 octahedra tilt as a result of non-ideal size or other factors, including strain on the B-X bonds. Reprinted with permission from Chen et al.[11] Copyright 2015 Elsevier Inc.

(D) Phase change of $MAPbI_3$ with different temperatures. Reprinted with permission from Stoumpos et al.[76] Copyright 2013 American Chemical Society.

With the strategy of mixed halides, the optoelectronic properties of perovskite can be tuned. It seems that the A^+ component plays a more important role in determining the stability of the crystal structures, given that replacing MA with Cs^+, FA^+, or mixed cations improved the stability of perovskites under conditions such as humidity, light irradiance, and heat. Chemically tailoring the perovskite films will require further exploration of the perovskite material systems to improve optoelectronic properties and chemical robustness.[80,81]

Several different device architectures of PSCs have been investigated. Initially, the first PSC by Kojima et al. was similar to the liquid-based DSSC in which the perovskite material functioned as the light absorber.[9] After this work, Park and colleagues[82] demonstrated a solid-state perovskite DSSC with a solid-state spiro-oMeTAD small-molecule hole transport layer. Later, a deeper understanding of the working mechanisms was unveiled by the observation that replacing the TiO_2 with insulating Al_2O_3 can also lead to efficient solar cells as a result of the good charge-transporting properties of perovskite. This led to the possibility of versatile PSC structures beyond the DSSC picture. A further evolution in device architecture was the planar heterojunction PSC, in which perovskite functions as both a light absorber and a bipolar charge transporter.[83] The similarity between PSCs and organic solar cells in device architecture has allowed a large amount of successful experiences in organic

Table 3. Crystallographic Data of Various Hybrid Perovskites

	Phase	Structure	Lattice Parameters (Å)			Volume (Å)
$MAPbI_3$	α	tetragonal	a = 6.3115	b = 6.3115	c = 6.3161	251.6
$MAPbI_3$	β	tetragonal	a = 8.849	b = 8.849	c = 12.642	990
$MAPbI_3$	γ	orthorhombic	a = 5.673	b = 5.628	c = 11.182	959.6
$MAPbCl_3$	α	cubic	a = 5.675	–	–	182.2
$MAPbCl_3$	β	tetragonal	a = 5.655	–	c = 5.630	180.1
$MAPbCl_3$	γ	orthorhombic	a = 5.673	b = 5.628	c = 11.182	375
$MAPbBr_3$	α	cubic	a = 5.901	–	–	206.3
$MAPbBr_3$	β	tetragonal	a = 8.322	–	c = 11.833	819.4
$MAPbBr_3$	γ	tetragonal	a = 5.8942	–	c = 5.8612	–
$MAPbBr_3$	δ	orthorhombic	a = 7.979	b = 8.580	c = 11.849	811.1
$MASnI_3$	α	tetragonal	a = 6.2302	b = 6.2302	c = 6.2316	241.88
$MASnI_3$	β	tetragonal	a = 8.7577	b = 8.7577	c = 12.429	953.2
$FAPbI_3$	α	trigonal	a = 8.9817	b = 8.9817	c = 11.006	768.9
$FAPbI_3$	β	trigonal	a = 17.791	b = 17.791	c = 10.091	2,988.4
$FASnI_3$	α	orthorhombic	a = 6.3286	b = 8.9554	c = 8.9463	507.03
$FASnI_3$	β	orthorhombic	a = 12.512	b = 12.512	c = 12.509	1,959.2

solar cells, e.g., solution-processed interfacial layers, to be applied to PSCs.[84] Both the planar heterojunction and mesoporous structures show high device performance, but different behaviors were observed in other aspects, e.g., the hysteresis, stability, etc. (Figure 11).[85]

The performance of PSC devices critically depends on the film-formation process. Specific requirements of the perovskite film active layer in PSCs include homogeneity and crystallinity. Thus, a variety of processing methods have been developed to control the dynamics or kinetics of the crystallization process, mainly including one-step or two-step sequential deposition methods based on the solution process,[86] the vacuum deposition,[87] or the vapor-assisted solution process.[88] For the solution-processed one-step method, the A, B, and X components are mixed in a single solution in a stoichiometric ratio, spun to form a homogeneous film, and converted into a solid perovskite phase by heating. As a result, the crystallization process is controlled by the nucleation process. Studies on the precursor solution indicate that these precursors form colloidal structures within the solution. Thereafter, a variety of methods, such as additives, solvent engineering, substrate modification, and hot injection, have been developed to control film formation. For the two-step method, one of the precursors is deposited first, and another is sequentially deposited on top via spin coating, dip coating, or a vapor-assisted process, and the perovskite film is formed spontaneously by heating. In this process, the diffusion of precursors controls the crystallization process. One of the most important factors for achieving high-quality perovskite films for photovoltaic devices is that a highly homogeneous and crystalline film is formed, which correlates to a high-quality initial PbI_2 film in the two-step procedure.

The extraordinary performances of PSCs stem from the substantial characteristic properties of the perovskite active layer, which delivers a strong optical absorption, an adjustable band gap, long diffusion lengths, ambipolar charge transport, high carrier mobility, and a high defect tolerance. The absorption coefficient of perovskite is measured to be 10^4–10^6 cm^{-1}, which is comparable to that of GaAs. Stranks

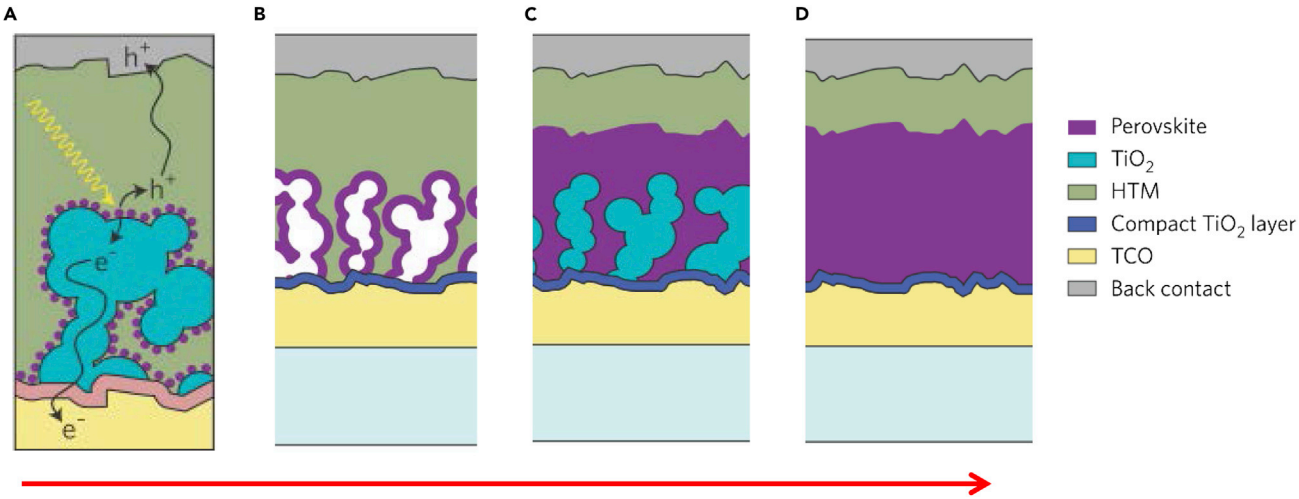

Figure 11. Typical Device Architecture of PSCs

(A) Perovskite materials working as only light absorbers, similar to the dyes in DSSCs.

(B) Perovskite materials working as both light absorbers and electron transporters.

(C) Perovskite materials working as both light absorbers and hole transporters.

(D) Planar heterojunction structure with perovskite materials as light absorbers and carrier transporters.

Reprinted by permission from Macmillan Publishers Ltd: Nature Materials (Grätzel[84]), copyright 2014.

et al.[89] and Xing et al.[90] have synchronously shown that carrier diffusion lengths of perovskites can reach up to the micrometer level with bipolar charge-transport properties (Figure 12A). Further enhanced diffusion lengths of 175 μm have been reported in single crystals.[89] In a study on laser-flash time-resolved microwave conductivity, Oga et al. demonstrated that the trap states in perovskite films is rather shallow.[92] In addition, PSCs show a good maximum photon-energy-utilization efficiency (i.e., a small difference between the open-circuit voltage and the band gap). The origin of the extraordinary optoelectronic properties of perovskites is still under investigation, and one of the possible explanations is the shielding effect,[93] where the polar effect of the MA^+ molecule protects a polaron from recombining. However, a strong hysteresis effect on the photocurrent-voltage curves poses a severe problem in accurate measurement of device performance, which casts doubt on the reported device efficiencies obtained by simple scans of I-V curves (Figure 12B).[91] It has been observed that hysteresis is related to abundant factors, e.g., the existence of a mesoporous scaffold, interfacial layers, perovskite morphology, charge accumulation, and ion migration. Among possible causes, ion migration due to the ionic nature of the perovskite crystal is one of the strongest candidates. The accumulation of different ionic species adjacent to the electrodes induces p- or n-doping in the perovskite layer near the charge-collection layers and affects the built-in potential of the device. Establishing a reliable characterization platform to accurately measure real device performance will require further insight into hysteresis. Some possible strategies include interfacial engineering, surface passivation, and morphology control.

Another critical issue with PSCs is device stability (Figure 12C). It has been reported that perovskite tends to decompose under heat, moisture,[94] and even illumination.[95] Industrial testing requires that solar cells survive under temperatures ranging from −40°C to 85°C for several years. However, it has been demonstrated that even the $MAPbI_3$ layers tend to decompose completely into PbI_2 on a 150°C hot plate

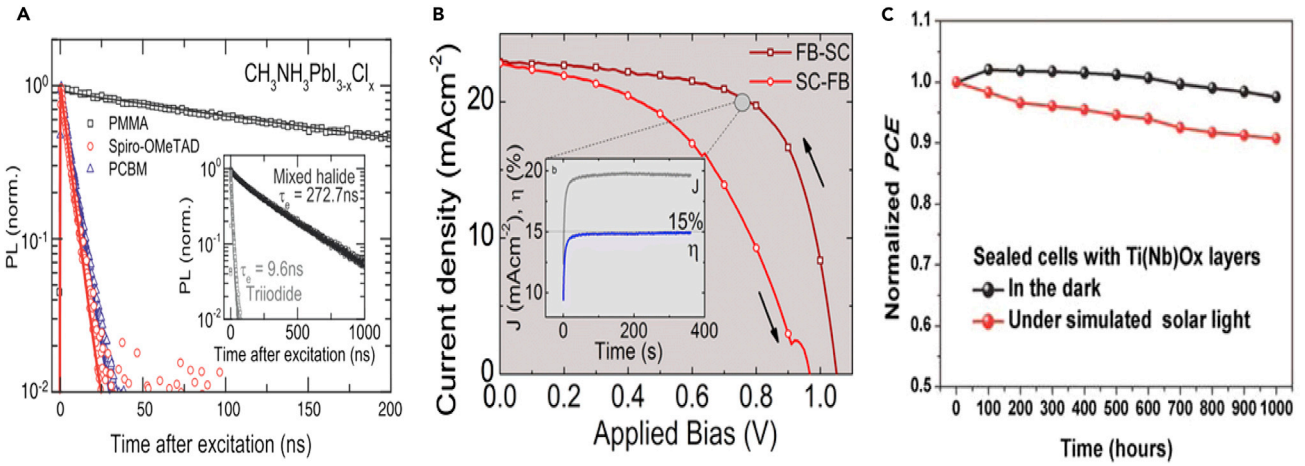

Figure 12. Optoelectrical Properties of PSCs

(A) Transient photoluminescence of MAPbI3-xClx. From Stranks et al.[89] Reprinted with permission from AAAS.

(B) The current densities of forward scans and reverse scans have large hysteresis. Reprinted with permission from Snaith et al.[91] Copyright 2014 American Chemical Society.

(C) Stability issue of PSCs. The PCE of PSCs degrades as time passes. From Chen et al.[85] Reprinted with permission from AAAS.

within 60 min. Thermal stability relies on the intrinsic properties of the perovskite film and can potentially be addressed or alleviated by a change in material composition, e.g., replacing MA^+ with FA^+ or Cs^+ or replacing I^- with SCN^-.[96]

Nevertheless, the progress of PSCs has proceeded rapidly. Thus far, certified record efficiencies up to 22% have been demonstrated, showing that PSCs are promising competition for their silicon-based counterparts.[60] Therefore, the development of materials, e.g., compositional engineering, advancements in processing, and evolution of interfacial charge-transporting materials, will boost PSCs toward a more feasible technique for practical application.

OUTLOOK AND CONCLUSION

Powering satellites with solar cells has led to big changes in our world. However, the ability to power terrestrial applications with solar technology has the potential to have an even larger impact. In the past few decades, the solar field has seen much progress pertaining to the advancement of solution-processible solar cells because they possess the capability to drastically reduce the cost of solar cells to a level comparable to that of fossil fuels.

On the other hand, although progress in solution-processible solar cells is exciting, still many hurdles must be overcome before commercialization can become a reality. For example, ensuring good inter-chain interaction and crystallinity is still an issue in achieving high-performance organic solar cells. In addition, there is a high necessity for the design of novel p-type polymers that are compatible with a series of n-type polymers and yield good performance through simple and cost-effective processing. Reducing photovoltage loss in solar energy conversion and stability are two of the largest challenges that the OPV field is facing. Solution-processible chalcogenide-based solar cells (CIGS and CZTS) accompany the toxicity and extensive reactivity of hydrazine despite its promise of high performance. In addition, during selenization, it is challenging to control phase purity and uniformity, which affect

charge recombination. Likewise, hybrid PSCs still suffer from critical issues in hysteresis and instability, despite the rapid progress in improving device performance and our fundamental understanding of this material. Also, the toxicity of lead elements is another crucial challenge.

Despite the issues remaining in solution-processible solar cells, they have certainly made great contributions to the development of the solar field. In particular, the cost effectiveness of solution-based processes, which avoid the necessity for high-vacuum processes, is highly appealing. Although this review focuses only on single-junction solar cells, all of these solution-processible solar technologies can be easily integrated into tandem configurations with light-management technologies to further enhance solar cell efficiency. In solving the remaining issues, solution-processible solar cells might finally be able to bring forth a bright future for affordable and efficient terrestrial solar technologies.

AUTHOR CONTRIBUTIONS

Y.Y. and G.L. conceptualized the article contents and supervised the preparation of the manuscript. S.-H.B., H.Z., Y.-T.H., and L.Z. equally contributed to writing the following main sections: Introduction, Solution-Processible Thin-Film Solar Cells, and Outlook and Conclusion. G.L., S.-H.B., N.D.M., and Y.S.R. are responsible for revising and integrating the article.

ACKNOWLEDGMENTS

This work is supported by the National Science Foundation (grant CHE-1230598 to program manager Linda S. Sapochak; grant ECCS-1202231 to program manager Radhakisan S. Baheti), the Air Force Office of Scientific Research (grant FA9550-15-1-0333 to program manager Charles Lee), and the Office of Naval Research (grant N00014-14-1-0648 to program manager Paul Armistead).

REFERENCES AND NOTES

1. International Energy Agency (2015). World Energy Outlook 2015, http://www.worldenergyoutlook.org/weo2015/.

2. Chapin, D.M., Fuller, C., and Pearson, G. (1954). A new silicon p-n junction photocell for converting solar radiation into electrical power. J. Appl. Phys. *25*, 676–677.

3. Carlson, D.E., and Wronski, C.R. (1976). Amorphous silicon solar cell. Appl. Phys. Lett. *28*, 671–673.

4. Bonnet, D., and Rabenhorst, H. (1972). New results on the development of a thin-film p-CsTe n-CdS heterojunction solar cell. Proceedings of the 9th Photovoltaic Specialists Conference, pp. 129–132.

5. Shay, J., Wagner, S., Bachmann, K., Buehler, E., and Kasper, H. (1975). Proceedings of the 11th Photovoltaic Specialists Conference, pp. 503–507.

6. Tang, C.W. (1986). Two-layer organic photovoltaic cell. Appl. Phys. Lett. *48*, 183–185.

7. Chirilă, A., Reinhard, P., Pianezzi, F., Bloesch, P., Uhl, A.R., Fella, C., Kranz, L., Keller, D., Gretener, C., Hagendorfer, H., et al. (2013). Potassium-induced surface modification of Cu(In,Ga)Se2 thin films for high-efficiency solar cells. Nat. Mater. *12*, 1107–1111.

8. O'Regan, B.,, and Grätzel, M. (1991). A low-cost, high-efficiency solar cell based on dye-sensitized colloidal TiO_2 films. Nature *353*, 737–740.

9. Kojima, A., Teshima, K., Shirai, Y., and Miyasaka, T. (2009). Organometal halide perovskites as visible-light sensitizers for photovoltaic cells. J. Am. Chem. Soc. *131*, 6050–6051.

10. Halls, J.J.M., Walsh, C.A., Greenham, N.C., Marseglia, E.A., Friend, R.H., Moratti, S.C., and Holmes, A.B. (1995). Efficient photodiodes from interpenetrating polymer networks. Nature *376*, 498–500.

11. Chen, Q., De Marco, N., Yang, Y., Song, T.-B., Chen, C.-C., Zhao, H., Hong, Z., Zhou, H., and Yang, Y. (2015). Under the spotlight: The organic–inorganic hybrid halide perovskite for optoelectronic applications. Nano Today *10*, 355–396.

12. Nelson, J. (2003). The Physics of Solar Cells, *Volume 1* (World Scientific).

13. Alharbi, F.H., Rashkeev, S.N., El-Mellouhi, F., Lüthi, H.P., Tabet, N., and Kais, S. (2015). An efficient descriptor model for designing materials for solar cells. npj Computational Materials *1*, 15003.

14. Munday, J.N. (2012). The effect of photonic bandgap materials on the Shockley-Queisser limit. J. Appl. Phys. *112*, 064501.

15. Shockley, W., and Queisser, H.J. (1961). Detailed Balance Limit of Efficiency of p-n Junction Solar Cells. J. Appl. Phys. *32*, 510–519.

16. Dou, L., You, J., Hong, Z., Xu, Z., Li, G., Street, R.A., and Yang, Y. (2013). 25th anniversary article: a decade of organic/polymeric photovoltaic research. Adv. Mater. *25*, 6642–6671.

17. Li, G., Zhu, R., and Yang, Y. (2012). Polymer solar cells. Nat. Photonics *6*, 153–161.

18. Lu, L., Zheng, T., Wu, Q., Schneider, A.M., Zhao, D., and Yu, L. (2015). Recent advances in bulk heterojunction polymer solar cells. Chem. Rev. *115*, 12666–12731.

19. Bao, Z., Dodabalapur, A., and Lovinger, A.J. (1996). Soluble and processable regioregular poly(3-hexylthiophene) for thin film field-effect transistor applications with high mobility. Appl. Phys. Lett. *69*, 4108–4110.

20. Morin, F.J., and Maita, J.P. (1954). Electrical properties of silicon containing arsenic and boron. Phys. Rev. *96*, 28–35.

21. Tamao, K., Sumitani, K., and Kumada, M. (1972). Selective carbon-carbon bond

formation by cross-coupling of Grignard reagents with organic halides. Catalysis by nickel-phosphine complexes. J. Am. Chem. Soc. *94*, 4374–4376.

22. Stille, J.K. (1986). The palladium-catalyzed cross-coupling reactions of organotin reagents with organic electrophiles. Angew. Chem. Int. Ed. Engl. *25*, 508–524.

23. Miyaura, N., and Suzuki, A. (1995). Palladium-catalyzed cross-coupling reactions of organoboron compounds. Chem. Rev. *95*, 2457–2483.

24. Sariciftci, N.S., Smilowitz, L., Heeger, A.J., and Wudl, F. (1992). Photoinduced electron transfer from a conducting polymer to buckminsterfullerene. Science *258*, 1474–1476.

25. Armstrong, N.R., Wang, W., Alloway, D.M., Placencia, D., Ratcliff, E., and Brumbach, M. (2009). Organic/Organic' heterojunctions: organic light emitting diodes and organic photovoltaic devices. Macromol. Rapid Commun. *30*, 717–731.

26. Forrest, S.R. (1997). Ultrathin organic films grown by organic molecular beam deposition and related techniques. Chem. Rev. *97*, 1793–1896.

27. Yu, G., Gao, J., Hummelen, J.C., Wudl, F., and Heeger, A.J. (1995). Polymer photovoltaic cells: enhanced efficiencies via a network of internal donor-acceptor heterojunctions. Science *270*, 1789–1791.

28. Wudl, F. and Srdanov, G. February 1993. US patent 5,189,136. https://www.google.com/patents/US5189136.

29. Wessling, R.A., and Zimmerman, R.G. September 1968. US patent 3,401,152. https://www.google.com/patents/US3401152.

30. Gilch, H.G., and Wheelwright, W.L. (1966). Polymerization of α-halogenated p-xylenes with base. J. Polym. Sci. A1 *4*, 1337–1349.

31. McCullough, R.D., and Lowe, R.D. (1992). Enhanced electrical conductivity in regioselectively synthesized poly(3-alkylthiophenes). J. Chem. Soc. Chem. Commun. *1992*, 70–72.

32. Li, G., Shrotriya, V., Huang, J., Yao, Y., Moriarty, T., Emery, K., and Yang, Y. (2005). High-efficiency solution processable polymer photovoltaic cells by self-organization of polymer blends. Nat. Mater. *4*, 864–868.

33. Sun, Y., Cui, C., Wang, H., and Li, Y. (2011). Efficiency enhancement of polymer solar cells based on Poly(3-hexylthiophene)/Indene-C70 bisadduct via methylthiophene additive. Adv. Energy Mater. *1*, 1058–1061.

34. Li, Y. (2012). Molecular design of photovoltaic materials for polymer solar cells: toward suitable electronic energy levels and broad absorption. Acc. Chem. Res. *45*, 723–733.

35. Cheng, Y.-J., Yang, S.-H., and Hsu, C.-S. (2009). Synthesis of conjugated polymers for organic solar cell applications. Chem. Rev. *109*, 5868–5923.

36. Blouin, N., Michaud, A., and Leclerc, M. (2007). A low-bandgap Poly(2,7-Carbazole) derivative for use in high-performance solar cells. Adv. Mater. *19*, 2295–2300.

37. Hou, J., Chen, H.-Y., Zhang, S., Li, G., and Yang, Y. (2008). Synthesis, characterization, and photovoltaic properties of a low band gap polymer based on silole-containing polythiophenes and 2,1,3-benzothiadiazole. J. Am. Chem. Soc. *130*, 16144–16145.

38. Zhu, Z., Waller, D., Gaudiana, R., Morana, M., Mühlbacher, D., Scharber, M., and Brabec, C. (2007). Panchromatic conjugated polymers containing alternating donor/acceptor units for photovoltaic applications. Macromolecules *40*, 1981–1986.

39. Liang, Y., Xu, Z., Xia, J., Tsai, S.T., Wu, Y., Li, G., Ray, C., and Yu, L. (2010). For the bright future-bulk heterojunction polymer solar cells with power conversion efficiency of 7.4%. Adv. Mater. *22*, E135–E138.

40. Liang, Y., Wu, Y., Feng, D., Tsai, S.-T., Son, H.-J., Li, G., and Yu, L. (2009). Development of new semiconducting polymers for high performance solar cells. J. Am. Chem. Soc. *131*, 56–57.

41. Hou, J., Park, M.-H., Zhang, S., Yao, Y., Chen, L.-M., Li, J.-H., and Yang, Y. (2008). Bandgap and molecular energy level control of conjugated polymer photovoltaic materials based on Benzo[1,2-b:4,5-b′]dithiophene. Macromolecules *41*, 6012–6018.

42. Dou, L., You, J., Yang, J., Chen, C.-C., He, Y., Murase, S., Moriarty, T., Emery, K., Li, G., and Yang, Y. (2012). Tandem polymer solar cells featuring a spectrally matched low-bandgap polymer. Nat. Photonics *6*, 180–185.

43. You, J., Dou, L., Yoshimura, K., Kato, T., Ohya, K., Moriarty, T., Emery, K., Chen, C.-C., Gao, J., Li, G., and Yang, Y. (2013). A polymer tandem solar cell with 10.6% power conversion efficiency. Nat. Commun. *4*, 1446.

44. Nguyen, T.L., Choi, H., Ko, S.J., Uddin, M.A., Walker, B., Yum, S., Jeong, J.E., Yun, M.H., Shin, T.J., Hwang, S., et al. (2014). Semi-crystalline photovoltaic polymers with efficiency exceeding 9% in a ~300 nm thick conventional single-cell device. Energy Environ. Sci. *7*, 3040.

45. Vohra, V., Kawashima, K., Kakara, T., Koganezawa, T., Osaka, I., Takimiya, K., and Murata, H. (2015). Efficient inverted polymer solar cells employing favourable molecular orientation. Nat. Photonics.

46. Chen, Z., Cai, P., Chen, J., Liu, X., Zhang, L., Lan, L., Peng, J., Ma, Y., and Cao, Y. (2014). Low band-gap conjugated polymers with strong interchain aggregation and very high hole mobility towards highly efficient thick-film polymer solar cells. Adv. Mater. *26*, 2586–2591.

47. Liu, Y., Zhao, J., Li, Z., Mu, C., Ma, W., Hu, H., Jiang, K., Lin, H., Ade, H., and Yan, H. (2014). Aggregation and morphology control enables multiple cases of high-efficiency polymer solar cells. Nat. Commun. *5*, 5293.

48. Zhao, J., Li, Y., Yang, G., Jiang, K., Lin, H., Ade, H., Ma, W., and Yan, H. (2016). Efficient organic solar cells processed from hydrocarbon solvents. Nature Energy *1*, 15027.

49. Zhao, W., Qian, D., Zhang, S., Li, S., Inganäs, O., Gao, F., and Hou, J. (2016). Fullerene-Free Polymer Solar Cells with over 11% Efficiency and Excellent Thermal Stability. Adv. Mater. *28*, 4734–4739.

50. Li, G., Yao, Y., Yang, H., Shrotriya, V., Yang, G., and Yang, Y. (2007). "Solvent Annealing" Effect in Polymer Solar Cells Based on Poly(3-hexylthiophene) and Methanofullerenes. Adv. Funct. Mater. *17*, 1636–1644.

51. Chen, W., Xu, T., He, F., Wang, W., Wang, C., Strzalka, J., Liu, Y., Wen, J., Miller, D.J., Chen, J., et al. (2011). Hierarchical nanomorphologies promote exciton dissociation in polymer/fullerene bulk heterojunction solar cells. Nano Lett. *11*, 3707–3713.

52. Mitchell, T.N. (1986). Transition-metal catalysis in organotin chemistry. J. Organomet. Chem. *304*, 1–16.

53. Suzuki, A. (1985). Organoboron compounds in new synthetic reactions. Pure Appl. Chem. *57*, 1749–1758.

54. Rudenko, A.E., Wiley, C.A., Stone, S.M., Tannaci, J.F., and Thompson, B.C. (2012). Semi-random P3HT analogs via direct arylation polymerization. J. Polym. Sci. A Polym. Chem. *50*, 3691–3697.

55. Kowalski, S., Allard, S., and Scherf, U. (2012). Synthesis of Poly(4,4-dialkyl-cyclopenta[2,1-b:3,4-b-bT analogsne-alt-2,1,3-benzothiadiazole) (PCPDTBT) in a Direct Arylation Scheme. ACS Macro Lett. *1*, 465–468.

56. Wagner, S. (1974). $CuInSe_2$/CdS heterojunction photovoltaic detectors. Appl. Phys. Lett. *25*, 434–435.

57. Polizzotti, A., Repins, I.L., Noufi, R., Wei, S.-H., and Mitzi, D.B. (2013). The state and future prospects of kesterite photovoltaics. Energy Environ. Sci. *6*, 3171–3182.

58. Chung, C.-H., Bob, B., Lei, B., Li, S.-H., Hou, W.W., and Yang, Y. (2013). Hydrazine solution-processed CuIn(Se,S)2 thin film solar cells: Secondary phases and grain structure. Sol. Energy Mater. Sol. Cells *113*, 148–152.

59. Wang, W., Winkler, M.T., Gunawan, O., Gokmen, T., Todorov, T.K., Zhu, Y., and Mitzi, D.B. (2014). Device characteristics of CZTSSe thin-film solar cells with 12.6% efficiency. Adv. Energy Mater. *4*, 1301465.

60. National Center for Photovoltaics (2016) Best Research-Cell Efficiencies, http://www.nrel.gov/ncpv/images/efficiency_chart.jpg.

61. Panthani, M.G., Akhavan, V., Goodfellow, B., Schmidtke, J.P., Dunn, L., Dodabalapur, A., Barbara, P.F., and Korgel, B.A. (2008). Synthesis of CuInS2, CuInSe2, and Cu(InxGa(1-x))Se2 (CIGS) nanocrystal "inks" for printable photovoltaics. J. Am. Chem. Soc. *130*, 16770–16777.

62. Kaelin, M., Rudmann, D., and Tiwari, A.N. (2004). Low cost processing of CIGS thin film solar cells. Sol. Energy *77*, 749–756.

63. Jackson, P., Hariskos, D., Wuerz, R., Kiowski, O., Bauer, A., Friedlmeier, T.M., and Powalla, M. (2015). Properties of $Cu(In,Ga)Se^2$ solar cells with new record efficiencies up to 21.7%. Phys. Status Solidi RRL *9*, 28–31.

64. McLeod, S.M., Hages, C.J., Carter, N.J., and Agrawal, R. (2015). Synthesis and characterization of 15% efficient CIGSSe solar cells from nanoparticle inks. Prog. Photovolt. Res. Appl. *23*, 1550–1556.

65. Mitzi, D.B., Yuan, M., Liu, W., Kellock, A.J., Chey, S.J., Deline, V., and Schrott, A.G. (2008). A high-efficiency solution-deposited thin-film photovoltaic device. Adv. Mater. *20*, 3657–3662.

66. Chen, S., Gong, X.G., Walsh, A., and Wei, S.-H. (2009). Crystal and electronic band structure of Cu_2ZnSnX_4 (X=S and Se) photovoltaic absorbers: First-principles insights. Appl. Phys. Lett. *94*, 041903.

67. Guo, Q., Ford, G.M., Yang, W.-C., Walker, B.C., Stach, E.A., Hillhouse, H.W., and Agrawal, R. (2010). Fabrication of 7.2% efficient CZTSSe solar cells using CZTS nanocrystals. J. Am. Chem. Soc. *132*, 17384–17386.

68. Bag, S., Gunawan, O., Gokmen, T., Zhu, Y., Todorov, T.K., and Mitzi, D.B. (2012). Low band gap liquid-processed CZTSe solar cell with 10.1% efficiency. Energy Environ. Sci. *5*, 7060.

69. Chen, S., Walsh, A., Gong, X.G., and Wei, S.H. (2013). Classification of lattice defects in the kesterite Cu2ZnSnS4 and Cu2ZnSnSe4 earth-abundant solar cell absorbers. Adv. Mater. *25*, 1522–1539.

70. Walsh, A., Chen, S., Wei, S.-H., and Gong, X.-G. (2012). Kesterite thin-film solar cells: advances in materials modelling of Cu2ZnSnS4. Adv. Energy Mater. *2*, 400–409.

71. Guo, Q., Hillhouse, H.W., and Agrawal, R. (2009). Synthesis of Cu2ZnSnS4 nanocrystal ink and its use for solar cells. J. Am. Chem. Soc. *131*, 11672–11673.

72. Ki, W., and Hillhouse, H.W. (2011). Earth-abundant element photovoltaics directly from soluble precursors with high yield using a non-toxic solvent. Adv. Energy Mater. *1*, 732–735.

73. Jiang, C., Hsieh, Y.T., Zhao, H., Zhou, H., and Yang, Y. (2015). Controlling solid-gas reactions at nanoscale for enhanced thin film morphologies and device performances in solution-processed Cu2ZnSn(S,Se)4 solar cells. J. Am. Chem. Soc. *137*, 11069–11075.

74. Hodes, G. (2013). Applied physics. Perovskite-based solar cells. Science *342*, 317–318.

75. Green, M.A., Ho-Baillie, A., and Snaith, H.J. (2014). The emergence of perovskite solar cells. Nat. Photonics *8*, 506–514.

76. Stoumpos, C.C., Malliakas, C.D., and Kanatzidis, M.G. (2013). Semiconducting tin and lead iodide perovskites with organic cations: phase transitions, high mobilities, and near-infrared photoluminescent properties. Inorg. Chem. *52*, 9019–9038.

77. Li, C., Lu, X., Ding, W., Feng, L., Gao, Y., and Guo, Z. (2008). Formability of ABX3 (X = F, Cl, Br, I) halide perovskites. Acta Crystallogr. B *64*, 702–707.

78. Cao, D.H., Stoumpos, C.C., Farha, O.K., Hupp, J.T., and Kanatzidis, M.G. (2015). 2D homologous perovskites as light-absorbing materials for solar cell applications. J. Am. Chem. Soc. *137*, 7843–7850.

79. Im, J.-H., Luo, J., Franckevičius, M., Pellet, N., Gao, P., Moehl, T., Zakeeruddin, S.M., Nazeeruddin, M.K., Grätzel, M., and Park, N.-G. (2015). Nanowire perovskite solar cell. Nano Lett. *15*, 2120–2126.

80. Yin, W.-J., Yang, J.-H., Kang, J., Yan, Y., and Wei, S.-H. (2015). Halide perovskite materials for solar cells: a theoretical review. J. Mater. Chem. A. *3*, 8926–8942.

81. Eperon, G.E., Paternò, G.M., Sutton, R.J., Zampetti, A., Haghighirad, A.A., Cacialli, F., and Snaith, H.J. (2015). Inorganic caesium lead iodide perovskite solar cells. J. Mater. Chem. A. *3*, 19688–19695.

82. Kim, H.S., Lee, C.R., Im, J.H., Lee, K.B., Moehl, T., Marchioro, A., Moon, S.J., Humphry-Baker, R., Yum, J.H., Moser, J.E., et al. (2012). Lead iodide perovskite sensitized all-solid-state submicron thin film mesoscopic solar cell with efficiency exceeding 9%. Sci. Rep. *2*, 591.

83. Zhou, H., Chen, Q., Li, G., Luo, S., Song, T.B., Duan, H.-S., Hong, Z., You, J., Liu, Y., and Yang, Y. (2014). Photovoltaics. Interface engineering of highly efficient perovskite solar cells. Science *345*, 542–546.

84. Grätzel, M. (2014). The light and shade of perovskite solar cells. Nat. Mater. *13*, 838–842.

85. Chen, W., Wu, Y., Yue, Y., Liu, J., Zhang, W., Yang, X., Chen, H., Bi, E., Ashraful, I., Grätzel, M., and Han, L. (2015). Efficient and stable large-area perovskite solar cells with inorganic charge extraction layers. Science *350*, 944–948.

86. Im, J.-H., Kim, H.-S., and Park, N.-G. (2014). Morphology-photovoltaic property correlation in perovskite solar cells: One-step versus two-step deposition of CH3NH3PbI3. APL Mater. *2*, 081510.

87. Liu, M., Johnston, M.B., and Snaith, H.J. (2013). Efficient planar heterojunction perovskite solar cells by vapour deposition. Nature *501*, 395–398.

88. Chen, Q., Zhou, H., Hong, Z., Luo, S., Duan, H.-S., Wang, H.-H., Liu, Y., Li, G., and Yang, Y. (2014). Planar heterojunction perovskite solar cells via vapor-assisted solution process. J. Am. Chem. Soc. *136*, 622–625.

89. Stranks, S.D., Eperon, G.E., Grancini, G., Menelaou, C., Alcocer, M.J.P., Leijtens, T., Herz, L.M., Petrozza, A., and Snaith, H.J. (2013). Electron-hole diffusion lengths exceeding 1 micrometer in an organometal trihalide perovskite absorber. Science *342*, 341–344.

90. Xing, G., Mathews, N., Sun, S., Lim, S.S., Lam, Y.M., Grätzel, M., Mhaisalkar, S., and Sum, T.C. (2013). Long-range balanced electron- and hole-transport lengths in organic-inorganic CH3NH3PbI3. Science *342*, 344–347.

91. Snaith, H.J., Abate, A., Ball, J.M., Eperon, G.E., Leijtens, T., Noel, N.K., Stranks, S.D., Wang, J.T.-W., Wojciechowski, K., and Zhang, W. (2014). Anomalous hysteresis in perovskite solar cells. J. Phys. Chem. Lett. *5*, 1511–1515.

92. Oga, H., Saeki, A., Ogomi, Y., Hayase, S., and Seki, S. (2014). Improved understanding of the electronic and energetic landscapes of perovskite solar cells: high local charge carrier mobility, reduced recombination, and extremely shallow traps. J. Am. Chem. Soc. *136*, 13818–13825.

93. Zhu, X.Y., and Podzorov, V. (2015). Charge carriers in hybrid organic-inorganic lead halide perovskites might be protected as large polarons. J. Phys. Chem. Lett. *6*, 4758–4761.

94. You, J., Meng, L., Song, T.-B., Guo, T.-F., Yang, Y.M., Chang, W.-H., Hong, Z., Chen, H., Zhou, H., Chen, Q., et al. (2016). Improved air stability of perovskite solar cells via solution-processed metal oxide transport layers. Nat. Nanotechnol. *11*, 75–81.

95. Mei, A., Li, X., Liu, L., Ku, Z., Liu, T., Rong, Y., Xu, M., Hu, M., Chen, J., Yang, Y., et al. (2014). A hole-conductor-free, fully printable mesoscopic perovskite solar cell with high stability. Science *345*, 295–298.

96. Eperon, G.E., Stranks, S.D., Menelaou, C., Johnston, M.B., Herz, L.M., and Snaith, H.J. (2014). Formamidinium lead trihalide: a broadly tunable perovskite for efficient planar heterojunction solar cells. Energy Environ. Sci. *7*, 982–988.